IJMMM International Journal of Minerals, Metallurgy and Materials 矿物冶金与材料学报（英文版）

Hydration reactivity difference between dicalcium silicate and tricalcium silicate revealed from structural and Bader charge analysis

Chongchong Qi, Xinhang Xu, and Qiusong Chen

Cite this article as:
Chongchong Qi, Xinhang Xu, and Qiusong Chen, Hydration reactivity difference between dicalcium silicate and tricalcium silicate revealed from structural and Bader charge analysis, *Int. J. Miner. Metall. Mater.*, 29(2022), No. 2, pp. 335-344. https://doi.org/10.1007/s12613-021-2364-5

International Journal of Minerals, Metallurgy and Materials
Volume 29, Number 2, February 2022, Page 335
https://doi.org/10.1007/s12613-021-2364-5

Hydration reactivity difference between dicalcium silicate and tricalcium silicate revealed from structural and Bader charge analysis

Chongchong Qi[1,2),✉], *Xinhang Xu*[1)], *and Qiusong Chen*[1)]

1) School of Resources and Safety Engineering, Central South University, Changsha 410083, China
2) School of Molecular Science, University of Western Australia, Perth 6009, Australia
(Received: 13 July 2021; revised: 12 October 2021; accepted: 13 October 2021)

Abstract: Cement hydration is the underlying mechanism for the strength development in cement-based materials. The structural and electronic properties of calcium silicates should be elucidated to reveal their difference in hydration reactivity. Here, we comprehensively compared β-C_2S and M3-C_3S and investigated their structural properties and Bader charge in the unit cell, during surface reconstruction and after single water adsorption via density functional theory. We identified different types of atoms in β-C_2S and M3-C_3S by considering the bonding characteristics and Bader charge. We then divided the atoms into the following groups: for β-C_2S, Ca and O atoms divided into two and four groups, respectively; for M3-C_3S, Ca, O, and Si atoms divided into four, four, and three groups, respectively. Results revealed that the valence electron distribution on the surface was more uniform than that on the unit cell, indicating that some atoms became more reactive after surface relaxation. During water adsorption, the electrons of β-C_2S and M3-C_3S were transferred from the surface to the adsorbed water molecules through position redistribution and bond formation/breaking. On this basis, we explained why β-C_2S and M3-C_3S had activity differences. A type of O atom with special bond characteristics (no O–Si bonds) and high reactivity existed in the unit cell of M3-C_3S. Bader charge analysis showed that the reactivity of Ca and O atoms was generally higher in M3-C_3S than in β-C_2S. Ca/O atoms had average valence electron numbers of 6.437/7.550 in β-C_2S and 6.481/7.537 in M3-C_3S. Moreover, the number of electrons gained by water molecules in M3-C_3S at the surface was higher than that in β-C_2S. The average variations in the valence electrons of H_2O on β-C_2S and M3-C_3S were 0.041 and 0.226, respectively. This study further explains the differences in the hydration reactivity of calcium silicates and would be also useful for the design of highly reactive and environmentally friendly cements.

Keywords: calcium silicates; Portland cement; hydration reactivity; first-principle calculations

1. Introduction

As an important cementitious material, ordinary Portland cement is widely used in many areas, such as civil engineering, water conservancy, and cemented paste backfill [1–4]. Though Portland cement remarkably contributes to global development, its production is quite energy intensive. For example, raw materials (i.e., limestone) should be heated up to 1400°C before cooling and grinding [5]. Consequently, around 5%–7% of global CO_2 emissions can be related to cement production [6]. As such, one of the most critical priorities of the cement industry is the development of environment-friendly cement by either increasing its hydration reactivity or decreasing its production temperature.

However, achieving these objectives is hindered by the poor understanding of the cement hydration mechanism, especially the difference in hydration reactivity. Ordinary Portland cement is mainly composed of dicalcium silicate (Ca_2SiO_4, C_2S, 15wt%–30wt%) and tricalcium silicate (Ca_3SiO_5, C_3S, 50wt%–70wt%) [7]. The hydration of C_2S and C_3S is the main reason for the strength development in cement-based materials [8–10]. Although the remarkable variation in the hydration reactivity of C_2S and C_3S has been widely explored [11–13], the reason for their different hydration reactivities remains poorly understood [14].

Two main types of methods, namely, experimental and theoretical studies, are used to investigate cement hydration. Zhang *et al.* [15] experimentally studied cement hydration by using a chemical shrinkage test to determine and simulate the hydration kinetics of cement at high temperature and high pressure. Wyrzykowski *et al.* [16] investigated the basic creep of early cement paste with respect to cement hydration. However, the accuracy of experimental studies relies heavily on the bulk characterization of C_2S and C_3S materials; consequently, the analysis at a single atom level becomes difficult. Moreover, the availability of high-resolution techniques limits experimental investigations [17–18]. As such, experimental knowledge about the reaction mechanism at the atomic level is limited.

Theoretical calculations are essential tools to reveal cement hydration [19]. As the main techniques in theoretical calculations, density functional theory (DFT) and molecular

✉ Corresponding author: Chongchong Qi E-mail: chongchong.qi@csu.edu.cn

dynamics (MD) have been widely used to investigate cement constituents and their hydration. For example, Durgun *et al.* [20] investigated the structure of calcium silicates and analyzed the effect of impurities. Qi *et al.* [21–22] and Zhang *et al.* [23–24] examined the surface properties of calcium silicates and single adsorption. Svenum *et al.* [25] explored the structure, hydration, and chloride ion entry in C–S–H through DFT calculations. Cement hydration has also been studied through many other theoretical calculations in terms of different aspects, such as the elastic and/or thermodynamic properties of major cement phases [26–27], the influence of impurity [7,28], and bulk water adsorption on cement surfaces [29]. However, C_2S and C_3S have yet to be compared comprehensively in terms of their hydration reactivity.

Overall, the literature is limited in at least the following ways: (1) differences between β-C_2S and M3-C_3S in the unit cell have not been well investigated and discussed; (2) Bader charge illustrating the reactivity and water adsorption mechanism has not been discussed comprehensively, such as in the unit cell, during surface reconstruction, and after water adsorption; and (3) a comprehensive comparison of low-index surfaces and single water adsorption of β-C_2S and M3-C_3S has not been conducted. To resolve these gaps, we comprehensively compared β-C_2S and M3-C_3S through structural and Bader charge analysis. We believed that this research could further explain the differences in the hydration reactivity of calcium silicates and had certain practical significance for the manipulation of hydration reactivity by using simple chemical approaches, such as impurity. Moreover, our findings could be useful for the design of highly reactive and environment-friendly cement.

2. Computational methods

DFT calculation was conducted using VASP version 5.4.4 with the projector augmented-wave (PAW) method [30–31]. In DFT calculation, efficiency and accuracy should be considered during the selection of the exchange-correlation potential (such as pseudopotential versus full-potential). In the current study, the Perdew–Burke–Ernzerhof (PBE) functional in the generalised gradient approximation (GGA) was selected after the comparison with PBE_{sol}-GGA [22,32–33]. A detailed comparison of PBE and PBE_{sol}-GGA is provided in Table S1 in Supporting Material.

The initial structures of β-C_2S and M3-C_3S were standardized in previous studies [34–35]. The selected valence electrons of H, O, Ca, and Si were $1s^1$, $2s^22p^4$, $3p^64s^2$, and $3s^23p^2$, respectively. After the full convergence test, 600 eV and 1.0×10^{-5} eV/atom were chosen as the energy cutoff and energy tolerance, respectively. Unit cell relaxation was stopped when the maximum residual force was less than 0.01 eV/Å on each atom. The k-points of β-C_2S and M3-C_3S were $4 \times 3 \times 2$ and $3 \times 4 \times 2$, respectively. In the unit cell, β-C_2S consisted of 4 Si atoms, 8 Ca atoms, and 16 O atoms, while M3-C_3S contained 6 Si atoms, 18 Ca atoms, and 30 O atoms.

Low-index surfaces were prepared using the optimized unit cells. The periodicity of in-plane crystals was preserved during slab model construction. All surfaces were retained to be stoichiometric and neutral to avoid polarizing electric fields effectively [36–37]. The covalent bond between silicon and oxygen was preserved during surface cutting because the breakage of the O–Si bond is energy intensive. When a low-index surface could be cut in multiple ways, the surface with the lowest energy was chosen. No symmetrical arrangement on the upper and lower surfaces was found because of the natural arrangement of atoms. During surface optimization, all atoms in the slab model could be relaxed while the lattice parameters were fixed. The maximum residual force per atom was 0.03 eV/Å for surface optimization, as suggested in previous studies [38–40]. Dipole correction was also employed during surface optimization and water adsorption.

The molecular and dissociative water adsorption of β-C_2S and M3-C_3S was investigated on all low-index surfaces. The initial structures of water adsorption on the β-C_2S (001) surface were provided in the supporting material as an example (Fig. S1) [22]. A single water molecule was molecularly or dissociatively placed on the relaxed surface. Afterward, the whole slab was relaxed using the same relaxation parameters. The van der Waals correction was also employed during water adsorption calculations, which has been proven to be important for water adsorption [41]. In the current study, DFT-D3, which outperforms DFT-D2 in terms of three-body interactions in local geometry, was employed [42].

The adsorption energy (E_{ad}) is calculated as follows:

$$E_{ad} = E_{total} - \gamma \times 2A - E_{water} \quad (1)$$

where E_{total} is the total energy of the slab after adsorption, γ is the surface energy, E_{water} is the energy of isolated water molecules in the vacuum [43], and A is the surface area of the slab. When E_{ad} is negative, adsorption is favored. The more negative E_{ad} is, the more favorable the adsorption will be [44–45].

Bader charge calculation is a reliable method for analyzing charge density [46–48]. In this method, the continuous electron density is divided into regions bounded by the minimum values of individual atomic charge densities [49–50]. Through DFT calculation, we obtained the valence electron information of each atom after calculation. The valence electron of each atom in the employed pseudopotential minus the calculated value is the corresponding Bader charge.

3. Results

3.1. Unit cells of β-C_2S and M3-C_3S

Fig. 1(a) and (b) illustrate the unit cells of β-C_2S and M3-C_3S, respectively. Bader charge analysis on β-C_2S showed the following Bader charges: 1.565 or 1.544 for Ca atoms, 3.111 for Si atoms, and −1.540 to −1.561 O atoms. For M3-C_3S, the following Bader charges were obtained: 1.535 to 1.488 for Ca atoms, 3.116 to 3.107 for Si atoms, and −1.406 to −1.570 for O atoms. Ca and Si atoms lost electrons, while O atoms gained electrons in the optimized unit cells.

Atoms in unit cells were classified into several types by

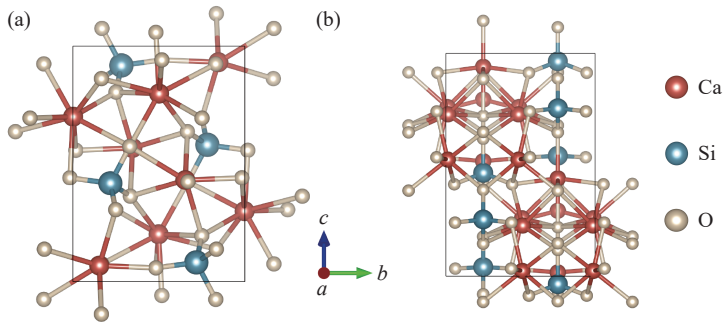

Fig. 1. Structure of unit cells: (a) β-C_2S and (b) M3-C_3S.

considering their Bader charge and bonding characteristics to present the difference in β-C_2S and M3-C_3S more clearly. Tables 1 and 2 summarize the atom types in β-C_2S. Ca, O, and Si had two, four, and one type in β-C_2S. For example, 16 O atoms in the unit cell were classified into four categories, namely, O_1 to O_4, with 4 O atoms in each category. Bonding type and Bader charge were considered during classification (i.e., O_1 and O_2 had the same bonding type but different Bader charges). Interestingly, the Si atom was bonded to four different types of O atoms in the SiO_4 tetrahedron (Fig. 2).

Tables 3–5 summarize the atom types in M3-C_3S. M3-C_3S had a more complex atomic structure in the unit cell. The Si atoms of M3-C_3S were classified into three types based on the Bader charge. O atoms were classified into four types based on Si types and bonding information. Among the four O types, O_1 had six Ca–O bonds, while O_2–O_4 had three or four Ca–O bonds and one Si–O bond. Ca atoms could be classified into four types.

3.2. Low-index surfaces of β-C_2S and M3-C_3S

Consistent with previous results [22], Fig. 3 shows the (001) surfaces of β-C_2S before and after optimization as an

Table 1. Classification of Ca atoms in β-C_2S

Type	Number of atoms	Bonding type (number of bonds)	Average Bader charge	Schematic
Ca_1	4	Ca_1–O_1 (1) Ca_1–O_2 (1) Ca_1–O_3 (2) Ca_1–O_4 (2)	1.544	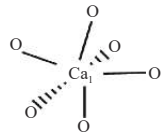
Ca_2	4	Ca_2–O_1 (2) Ca_2–O_2 (2) Ca_2–O_3 (2) Ca_2–O_4 (2)	1.565	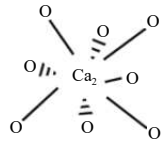

Table 2. Classification of O atoms in β-C_2S

Type	Number of atoms	Bonding type (number of bonds)	Average Bader charge	Schematic
O_1	4	O_1–Si (1) O_1–Ca_1 (1) O_1–Ca_2 (2)	−1.540	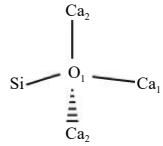
O_2	4	O_2–Si (1) O_2–Ca_1 (1) O_2–Ca_2 (2)	−1.558	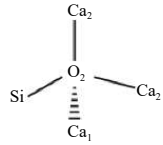
O_3	4	O_3–Si (1) O_3–Ca_1 (2) O_3–Ca_2 (2)	−1.556	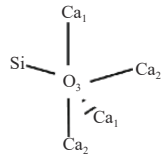
O_4	4	O_4–Si (1) O_4–Ca_1 (2) O_4–Ca_2 (2)	−1.561	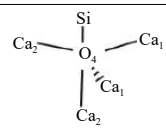

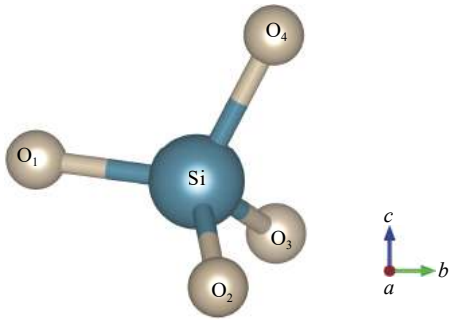

Fig. 2. Structural diagram of Si atom in β-C_2S.

example. As illustrated, surface atoms were redistributed in the *x*, *y*, and *z* directions after optimization. Chemical bonds were broken and formed. For example, the 6th Ca atom and the 15th O atom formed a new chemical bond after optimization, while the chemical bond between the 15th Ca atom and the 3rd O atom was broken. These results indicated that surface relaxation would not only shift the atomic positions but also create or break chemical bonds.

Fig. 4 shows the comparison of the valence electron distribution of low-index surfaces and unit cells. The valence electron distribution of the surface was more evenly distributed than that of the unit cell except for the valence electron distribution of O atoms in M3-C_3S, which was quite similar. For example, the peak of the surface distribution was much higher than that of the unit cell. This result indicated that the valence electron distribution on the surface was more uniform than that of the unit cell. With the implication of reactivity from Bader charge analysis [21,49], some surface atoms became more reactive after relaxation.

3.3. Single water molecule adsorption

Our previous study discussed the adsorption configura-

Table 3. Classification of Si atoms in M3-C_3S

Type	Number of atoms	Bonding type (number of bonds)	Average Bader charge	Schematic
Si_1	2	Si_1–O_2 (4)	3.114	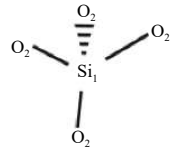
Si_2	2	Si_2–O_3 (4)	3.115	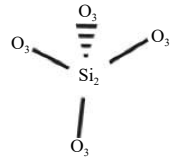
Si_3	2	Si_3–O_4 (4)	3.106	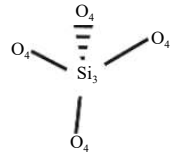

Table 4. Classification of O atoms in M3-C_3S

Type	Number of atoms	Bonding type (number of bonds)	Average Bader charge	Schematic
O_1	6	O_1–Ca (6)	−1.429	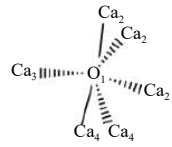
O_2	8	O_2–Si_1 (1) O_2–Ca (3)	−1.561	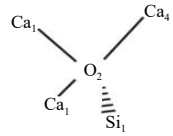
O_3	8	O_3–Si_2 (1) O_3–Ca (3)	−1.558	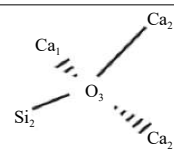
O_4	8	O_4–Si_3 (1) O_4–Ca (3 or 4)	−1.563	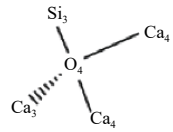

Table 5. Classification of Ca atoms in M3-C_3S

Type	Number of atoms (average Bader charge)	Bonding type (number of bonds)	Schematic
Ca_1	4 (1.518), 2 (1.524)	Ca_1–O_1 (2) Ca_1–O_2 (2) Ca_1–O_3 (1) Ca_1–O_4 (1)	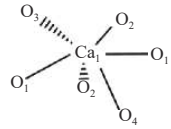
Ca_2	4 (1.535), 2 (1.488)	Ca_2–O_1 (2) Ca_2–O_2 (1) Ca_2–O_3 (2) Ca_2–O_4 (1)	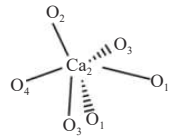
Ca_3	2 (1.520)	Ca_3–O_1 (2) Ca_3–O_2 (1) Ca_3–O_3 (1) Ca_3–O_4 (2)	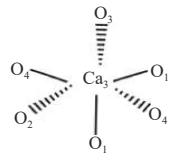
Ca_4	4 (1.529)	Ca_4–O_1 (2) Ca_4–O_2 (1) Ca_4–O_3 (1) Ca_4–O_4 (3)	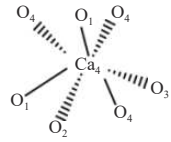

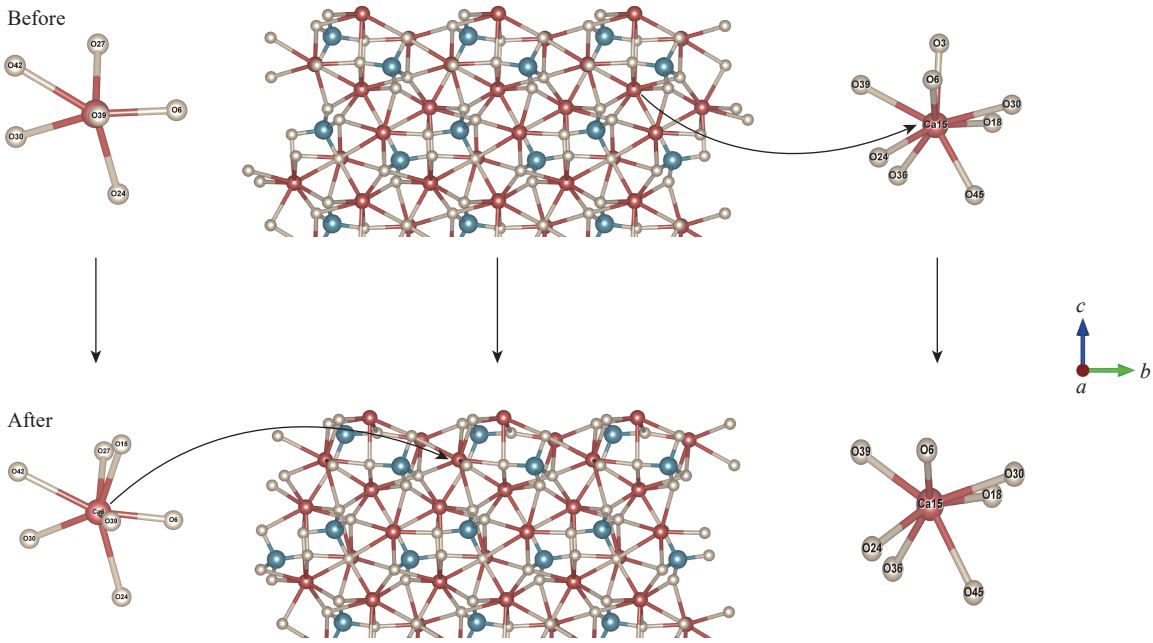

Fig. 3. (001) surface before and after β-C_2S optimization.

tion [22]. In the current study, the further structural analysis indicated that new bonds might be formed between surface atoms that were not directly involved in adsorption. Fig. 5 shows the structure of β-C_2S (001) before and after adsorption as an example. After water adsorption, the 3rd O atom created a new chemical bond with the 15th Ca atom below it. The same phenomenon was observed in several other surfaces of β-C_2S and M3-C_3S. These results demonstrated that water adsorption caused a more distinguishable reconfiguration of chemical bonds on the surface.

Fig. 6 illustrates the variation in the valence electrons of Ca, surface O ($O_{surface}$), water O (O_{water}), H_2O after water adsorption on β-C_2S and M3-C_3S. Only the surface atoms directly related to water adsorption were analyzed. The gain/loss of electrons ranged from −0.037 to 0.135 e^- for β-C_2S and −0.365 to 0.278 e^- for M3-C_3S. The valence electron of Ca and $O_{surface}$ atoms decreased after water adsorption, indicating that Ca and $O_{surface}$ atoms lost electrons. By contrast, O_{water} atoms and H_2O gained electrons. The electrons of β-C_2S and M3-C_3S transferred from the surface to the adsorbed water molecules. Electron transfer from the surface to absorbates, such as CO_2 adsorption on ceria (110) [51] and Ti_2C (111) [52], has also been widely described.

Fig. 7 illustrates the variation in the valence electrons of H_2O on β-C_2S and M3-C_3S surfaces whenever two adsorption configurations were observed [22]. The variation in valence electrons for dissociative adsorption was greater than that for molecular adsorption. Notably, the water molecule

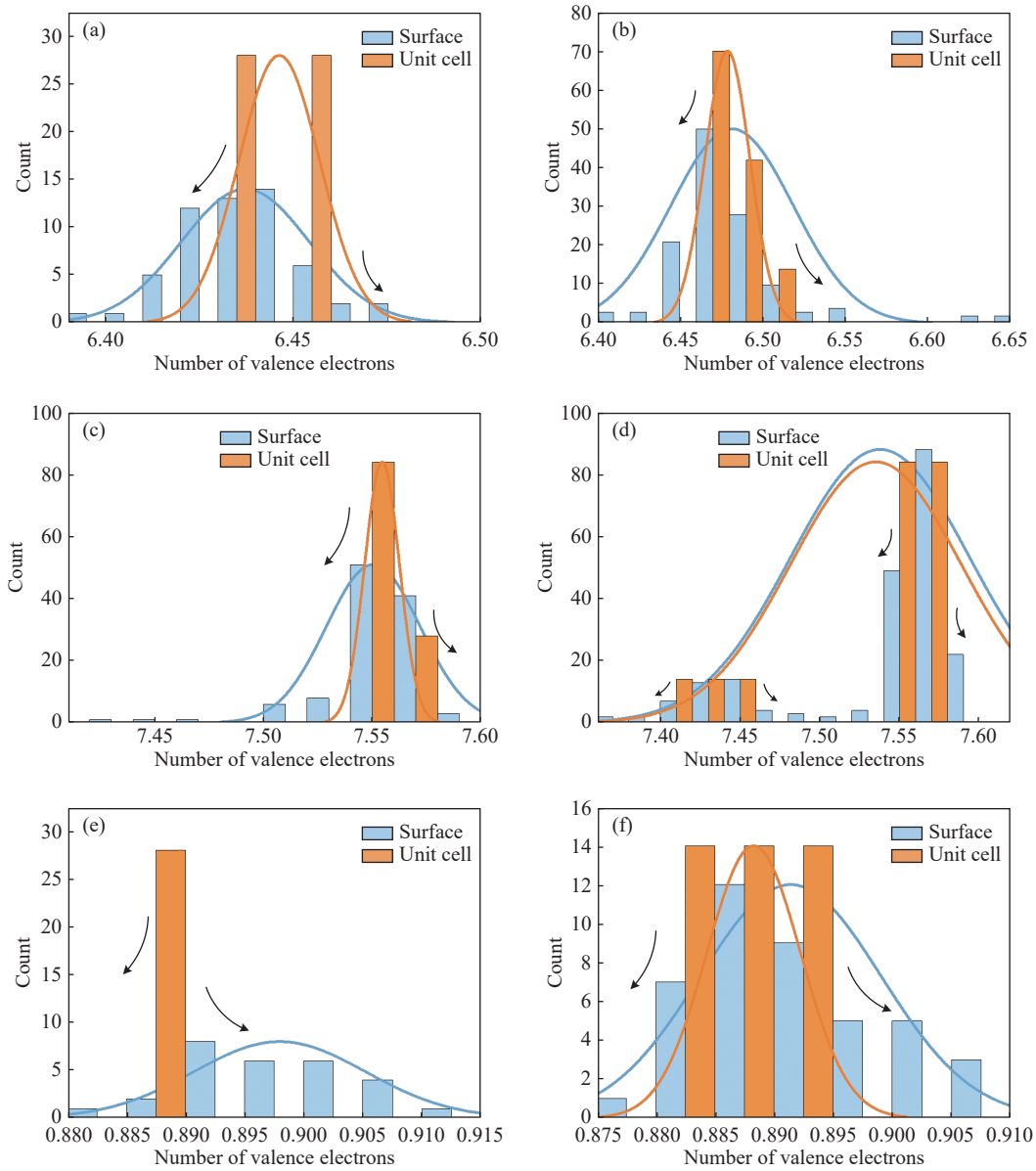

Fig. 4. Valence electron distribution of surfaces and unit cells: (a) Ca atoms of β-C_2S, (b) Ca atoms of M3-C_3S, (c) O atoms of β-C_2S, (d) O atoms of M3-C_3S, (e) Si atoms of β-C_2S, and (f) Si atoms of M3-C_3S. Note that one formula unit was considered during surface distribution calculation.

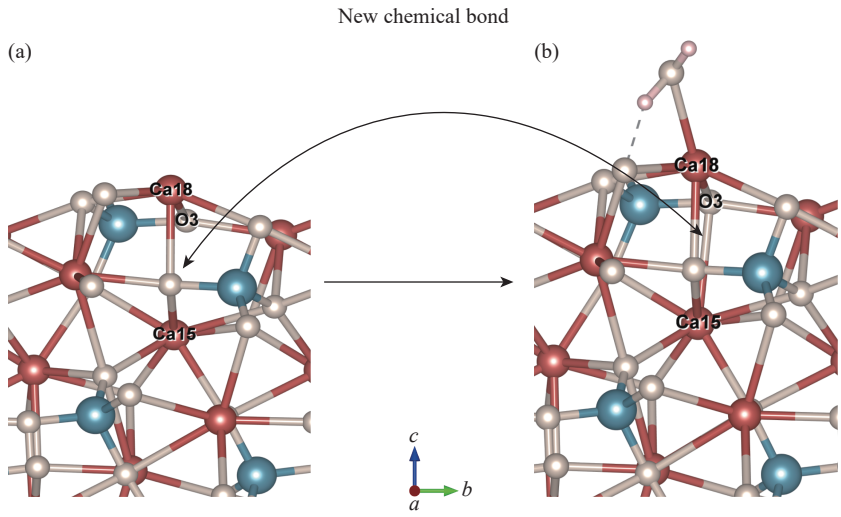

Fig. 5. Structure of the (001) surface of β-C_2S before (a) and after (b) surface adsorption.

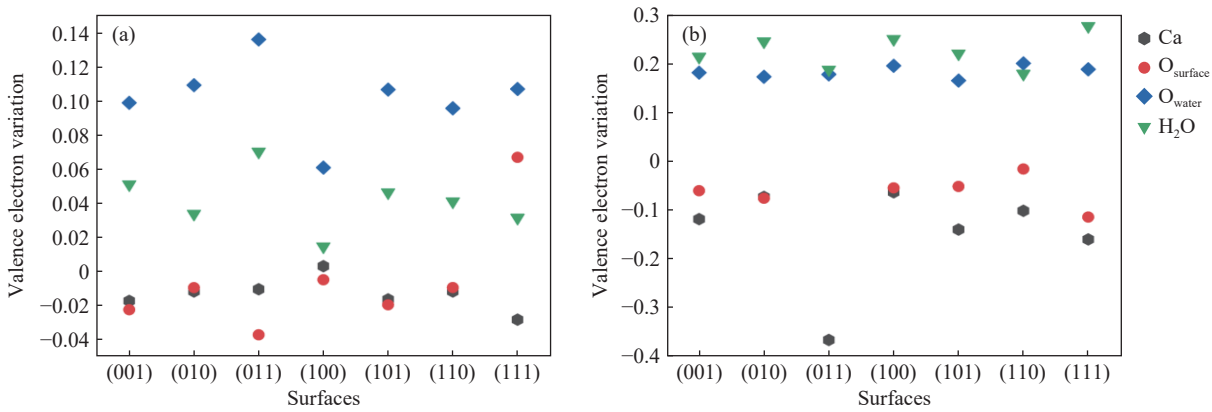

Fig. 6. Variation in valence electrons after and before water molecules adsorbed on the surface: (a) water molecules were adsorbed on the low-index surface of β-C_2S in a molecular form, and (b) water molecules were adsorbed on the low-index surface of M3-C_3S in a dissociated form.

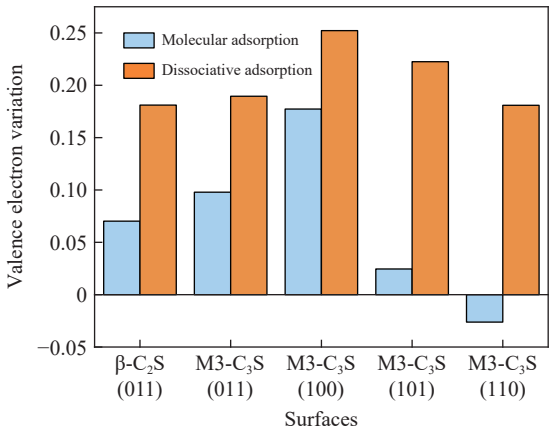

Fig. 7. Comparison of molecular and dissociative adsorption in terms of the variation in valence electrons of H_2O on β-C_2S and M3-C_3S surfaces.

lost electrons during molecular adsorption on the M3-C_3S surface, but this phenomenon should be investigated in future works.

4. Discussion

In this section, the difference between β-C_2S and M3-C_3S was discussed with potential implications for hydration reactivity.

4.1. Unit cell comparison of β-C_2S and M3-C_3S

Fig. 8 shows the valence electrons of Ca and O atoms in the unit cells of β-C_2S and M3-C_3S. The valence electrons of Ca atoms differed in β-C_2S and M3-C_3S. The number of the valence electrons of Ca atoms was higher in M3-C_3S than in β-C_2S, indicating the higher chemical reactivity of Ca atoms in M3-C_3S than in β-C_2S [21,49].

A significant difference was observed in the O atoms. A comparison between Tables 2 and 5 indicates a special type of O atom, i.e., the O_1 type in Table 5, in M3-C_3S. More specifically, the O_1 type in M3-C_3S was not chemically bonded to Si atoms. Moreover, the number of valence electrons of this type of O atom was 7.429, which was smaller than that of the other types of O atoms, indicating the higher reactivity of O_1 [21,49]. In M3-C_3S, each Ca was chemically bonded to two O atoms from the O_1 type. This special type of O atoms might also be the underlying cause of the higher reactivity of M3-C_3S.

This special type of O atoms in M3-C_3S, that without chemical bonding to Si atoms, has also been observed in other studies on the structural analysis of unit cells or surfaces [23,53–54]. Previous results further indicated the significance of our findings. For the first time, the current study comprehensively compared β-C_2S and M3-C_3S by considering structures and Bader charges. The results would be useful for

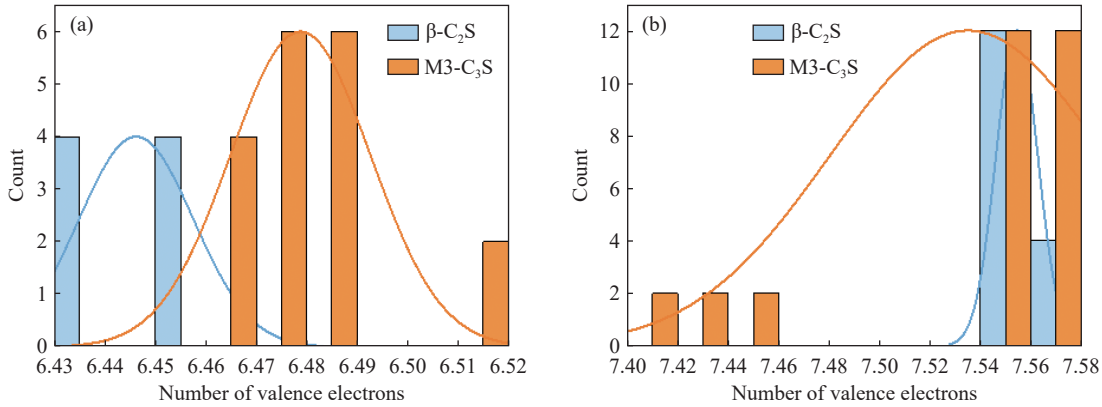

Fig. 8. Comparison of the valence electrons of unit cell atoms in β-C_2S and M3-C_3S: (a) Ca and (b) O atoms.

future discussions on β-C_2S and M3-C_3S.

4.2. Surface comparison of β-C_2S and M3-C_3S

Fig. 9 illustrates the comparison of the valence electrons of surface Ca/O atoms in β-C_2S and M3-C_3S after surface relaxation. The average numbers of valence electrons of Ca atoms in β-C_2S and M3-C_3S were 6.437 and 6.481, respectively, indicating that Ca atoms in M3-C_3S were more reactive than those in β-C_2S. Similar results were observed in O atoms. In terms of O atoms, the smaller the number of valence electrons, the higher the reactivity (7.550 in β-C_2S compared with 7.537 in M3-C_3S) [55–57]. The high reactivity of M3-C_3S could also be revealed by the largest/smallest number of valence electrons of Ca/O. For example, the smallest number of O valence electrons in M3-C_3S was 7.376, whereas that in β-C_2S was 7.437. These results indicated that the most reactive surface Ca/O sites in M3-C_3S were more reactive than those in β-C_2S. The surface comparison between β-C_2S and M3-C_3S further confirmed the high reactivity of M3-C_3S, which is consistent with the unit cell results.

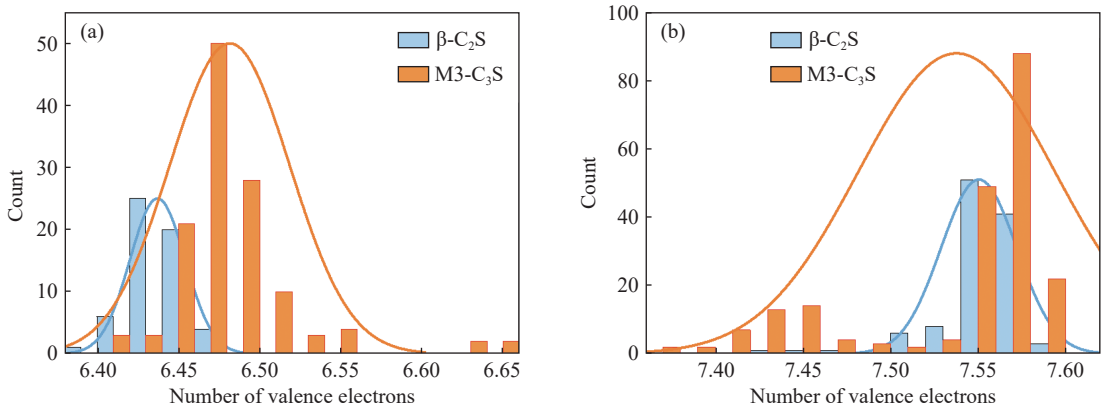

Fig. 9. Comparison of the valence electrons of surface atoms in β-C_2S and M3-C_3S: (a) Ca and (b) O atoms.

4.3. Water adsorption comparison of β-C_2S and M3-C_3S

Fig. 10 compares the valence electrons of H_2O on β-C_2S and M3-C_3S after adsorption. The average variations in the valence electrons of H_2O on β-C_2S and M3-C_3S were 0.041 and 0.226, respectively. These results indicated that the water molecule gained more electrons after its adsorption on M3-C_3S surfaces. Furthermore, the chemical reactivity of the M3-C_3S surface was higher than that of the β-C_2S surface.

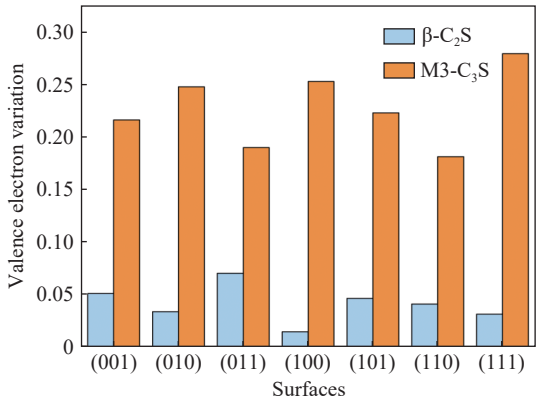

Fig. 10. Variation in the valence electrons of H_2O on β-C_2S and M3-C_3S after adsorption.

In future work, the hydration processes of multiple water molecules on cement surfaces should be investigated. The correlation between the reactivity and process of hydration should be further explained. The interaction between a large number of water molecules with cement surfaces should be investigated through molecular dynamics.

5. Conclusions

The unit cell, the low-index surfaces, and the adsorption of a single water molecule on surfaces were investigated through DFT calculations. Structural property and Bader charge analysis were performed to provide insights into the difference in the hydration reactivity of β-C_2S and M3-C_3S. Based on the results, the following conclusions could be drawn.

(1) In β-C_2S, Si, Ca, and O atoms were classified into one, two, and four types, respectively. In M3-C_3S, Ca, O, and Si were grouped into four, four, and three types, respectively.

(2) The valence electron distribution on the surface was more uniform than that on the unit cell, indicating that some atoms became more reactive after surface relaxation.

(3) Electrons were transferred from the surface to the water molecule. The gain/loss of electrons ranged from −0.037 e^- to 0.135 e^- for β-C_2S and from −0.365 e^- to 0.278 e^- for M3-C_3S.

(4) A special type of O atom was observed in the unit cell of M3-C_3S. It was not chemically bonded to Si atoms and had a smaller valence electron number of 7.429, which was smaller than that of other O types in β-C_2S and M3-C_3S.

(5) The reactivity of M3-C_3S atoms in the unit cell and surfaces was higher than that of β-C_2S. Moreover, the water molecules in M3-C_3S gained more electrons at the surface compared to β-C_2S.

Acknowledgements

This work was financially supported by the National Nat-

ural Science Foundation of China (No. 52004330). This work was also supported by resources provided by the Pawsey Supercomputing Centre with funding from the Australian Government and the Government of Western Australia.

Conflict of Interest

The authors declare that they have no conflict of interest.

Supplementary Information

The online version contains supplementary material available at https://doi.org/10.1007/s12613-021-2364-5

Additional file 1: Table S1. Lattice parameters of β-C_2S and M3-C_3S (experimental measurements and DFT calculations). **Fig. S1.** Initial structure of molecules and dissociative adsorption on the surface of β-C_2S (001): (a-1) molecular adsorption, (a-2) molecular adsorption, (b-1) dissociative adsorption, and (b-2) dissociative adsorption.

References

[1] J.Y. Huo, Z.J. Wang, T.H. Zhang, R. He, and H.X. Chen, Influences of interaction between cement and ionic paraffin emulsion on cement hydration, *Constr. Build. Mater.*, 299(2021), art. No. 123951.

[2] R. Li, L. Lei, T.B. Sui, and J. Plank, Effectiveness of PCE superplasticizers in calcined clay blended cements, *Cem. Concr. Res.*, 141(2021), art. No. 106334.

[3] S.H. Yin, L.M. Wang, X. Chen, and A.X. Wu, Agglomeration and leaching behaviors of copper oxides with different chemical binders, *Int. J. Miner. Metall. Mater.*, 28(2021), No. 7, p. 1127.

[4] Q.S. Chen, S.Y. Sun, Y.K. Liu, C.C. Qi, H.B. Zhou, and Q.L. Zhang, Immobilization and leaching characteristics of fluoride from phosphogypsum-based cemented paste backfill, *Int. J. Miner. Metall. Mater.*, 28(2021), No. 9, p. 1440.

[5] H.F. Taylor, *Cement Chemistry*, Thomas Telford, London, 1997, p. 1.

[6] J.M. Crow, The concrete conundrum, *Chem. World*, 5(2008), p. 62.

[7] J.P. Zhu, K. Yang, Y. Chen, G.X. Fan, L. Zhang, B.K. Guo, X.M. Guan, and R.Q. Zhao, Revealing the substitution preference of zinc in ordinary Portland cement clinker phases: A study from experiments and DFT calculations, *J. Hazard. Mater.*, 409(2021), art. No. 124504.

[8] B. Ercikdi, T. Yılmaz, and G. Külekci, Strength and ultrasonic properties of cemented paste backfill, *Ultrasonics*, 54(2014), No. 1, p. 195.

[9] I. Cavusoglu, E. Yilmaz, and A.O. Yilmaz, Sodium silicate effect on setting properties, strength behavior and microstructure of cemented coal fly ash backfill, *Powder Technol.*, 384(2021), p. 17.

[10] C.C. Qi and A. Fourie, Cemented paste backfill for mineral tailings management: Review and future perspectives, *Miner. Eng.*, 144(2019), art. No. 106025.

[11] Y. Briki, M. Zajac, M.B. Haha, and K. Scrivener, Impact of limestone fineness on cement hydration at early age, *Cem. Concr. Res.*, 147(2021), art. No. 106515.

[12] X.Y. Pang, W. Cuello Jimenez, and J. Singh, Measuring and modeling cement hydration kinetics at variable temperature conditions, *Constr. Build. Mater.*, 262(2020), art. No. 120788.

[13] R.H. Yang and T.S. He, Influence of liquid accelerators combined with mineral admixtures on early hydration of cement pastes, *Constr. Build. Mater.*, 295(2021), art. No. 123659.

[14] O. Linderoth, L. Wadsö, and D. Jansen, Long-term cement hydration studies with isothermal calorimetry, *Cem. Concr. Res.*, 141(2021), art. No. 106344.

[15] Y.G. Zhang, C. Bouillon, N. Vlasopoulos, and J.J. Chen, Measuring and modeling hydration kinetics of well cements under elevated temperature and pressure using chemical shrinkage test method, *Cem. Concr. Res.*, 123(2019), art. No. 105768.

[16] M. Wyrzykowski, K. Scrivener, and P. Lura, Basic creep of cement paste at early age—The role of cement hydration, *Cem. Concr. Res.*, 116(2019), p. 191.

[17] P. Lalan, A. Dauzères, L. De Windt, D. Bartier, J. Sammaljärvi, J.D. Barnichon, I. Techer, and V. Detilleux, Impact of a 70°C temperature on an ordinary Portland cement paste/claystone interface: An *in situ* experiment, *Cem. Concr. Res.*, 83(2016), p. 164.

[18] Z.D. Zhang and G.W. Scherer, Physical and chemical effects of isopropanol exchange in cement-based materials, *Cem. Concr. Res.*, 145(2021), art. No. 106461.

[19] S. Tontapha, N. Shinsuphan, W. Sang-Aroon, L. Temprom, S. Krongsuk, W. Jarernboon, P. Chindaprasirt, and V. Amornkitbamrung, A DFT study on electrocatalytic performance of 12CaO·7Al_2O_3 (C12A7) with electrolytic LiI applied in DSSCs, *Surf. Sci.*, 711(2021), art. No. 121864.

[20] E. Durgun, H. Manzano, P.V. Kumar, and J.C. Grossman, The characterization, stability, and reactivity of synthetic calcium silicate surfaces from first principles, *J. Phys. Chem. C*, 118(2014), No. 28, p. 15214.

[21] C.C. Qi, L. Liu, J.Y. He, Q.S. Chen, L.J. Yu, and P.F. Liu, Understanding cement hydration of cemented paste backfill: DFT study of water adsorption on tricalcium silicate (111) surface, *Minerals*, 9(2019), No. 4, art. No. 202.

[22] C.C. Qi, D. Spagnoli, and A. Fourie, DFT-D study of single water adsorption on low-index surfaces of calcium silicate phases in cement, *Appl. Surf. Sci.*, 518(2020), art. No. 146255.

[23] Y. Zhang, X.Y. Lu, D.S. Song, and S.B. Liu, The adsorption of a single water molecule on low-index C3S surfaces: A DFT approach, *Appl. Surf. Sci.*, 471(2019), p. 658.

[24] Y. Zhang, X.Y. Lu, Z. He, and D.S. Song, Molecular and dissociative adsorption of a single water molecule on a β-dicalcium silicate (100) surface explored by a DFT approach, *J. Am. Ceram. Soc.*, 101(2018), No. 6, p. 2428.

[25] I.H. Svenum, I.G. Ringdalen, F.L. Bleken, J. Friis, D. Höche, and O. Swang, Structure, hydration, and chloride ingress in C–S–H: Insight from DFT calculations, *Cem. Concr. Res.*, 129(2020), art. No. 105965.

[26] C.C. Qi, A. Fourie, Q.S. Chen, and P.F. Liu, Application of first-principles theory in ferrite phases of cemented paste backfill, *Miner. Eng.*, 133(2019), p. 47.

[27] N.L. Mai, N.H. Hoang, H.T. Do, M. Pilz, and T.T. Trinh, Elastic and thermodynamic properties of the major clinker phases of Portland cement: Insights from first principles calculations, *Constr. Build. Mater.*, 287(2021), art. No. 122873.

[28] C.C. Qi, Q.S. Chen, and A. Fourie, Role of Mg impurity in the water adsorption over low-index surfaces of calcium silicates: A DFT-D study, *Minerals*, 10(2020), No. 8, art. No. 665.

[29] J. Huang, B. Wang, Y.T. Yu, L. Valenzano, M. Bauchy, and G. Sant, Electronic origin of doping-induced enhancements of reactivity: Case study of tricalcium silicate, *J. Phys. Chem. C*, 119(2015), No. 46, p. 25991.

[30] G. Kresse and J. Hafner, *Ab initio* molecular dynamics for liquid metals, *Phys. Rev. B*, 47(1993), No. 1, p. 558.

[31] G. Kresse and J. Furthmüller, Efficiency of ab-initio total energy calculations for metals and semiconductors using a plane-wave basis set, *Comput. Mater. Sci.*, 6(1996), No. 1, p. 15.

[32] P. Giannozzi, S. Baroni, N. Bonini, M. Calandra, R. Car, C.

Cavazzoni, D. Ceresoli, G.L. Chiarotti, M. Cococcioni, I. Dabo, A. dal Corso, S. de Gironcoli, S. Fabris, G. Fratesi, R. Gebauer, U. Gerstmann, C. Gougoussis, A. Kokalj, M. Lazzeri, L. Martin-Samos, N. Marzari, F. Mauri, R. Mazzarello, S. Paolini, A. Pasquarello, L. Paulatto, C. Sbraccia, S. Scandolo, G. Sclauzero, A.P. Seitsonen, A. Smogunov, P. Umari, and R.M. Wentzcovitch, QUANTUM ESPRESSO: A modular and open-source software project for quantum simulations of materials, *J. Phys.: Condens. Matter*, 21(2009), No. 39, art. No. 395502.

[33] J.P. Perdew, K. Burke, and M. Ernzerhof, Generalized gradient approximation made simple, *Phys. Rev. Lett.*, 77(1996), No. 18, p. 3865.

[34] K.H. Jost, B. Ziemer, and R. Seydel, Redetermination of the structure of β-dicalcium silicate, *Acta Crystallogr. Sect. B Struct. Crystallogr. Cryst. Chem.*, 33(1977), No. 6, p. 1696.

[35] M.N. de Noirfontaine, F. Dunstetter, M. Courtial, G. Gasecki, and M. Signes-Frehel, Polymorphism of tricalcium silicate, the major compound of Portland cement clinker: 2. Modelling alite for Rietveld analysis, an industrial challenge, *Cem. Concr. Res.*, 36(2006), No. 1, p. 54.

[36] P.W. Tasker, The stability of ionic crystal surfaces, *J. Phys. C: Solid State Phys.*, 12(1979), No. 22, p. 4977.

[37] C. Noguera, Polar oxide surfaces, *J. Phys.: Condens. Matter*, 12(2000), No. 31, p. R367.

[38] S.J. Tjung, Q. Zhang, J.J. Repicky, S.F. Yuk, X.W. Nie, N.M. Santagata, A. Asthagiri, and J.A. Gupta, STM and DFT studies of CO_2 adsorption on O–Cu(100) surface, *Surf. Sci.*, 679(2019), p. 50.

[39] Z. Jiang, P. Qin, and T. Fang, Investigation on adsorption and decomposition of H_2S on Pd (100) surface: A DFT study, *Surf. Sci.*, 632(2015), p. 195.

[40] A. Lloyd, D. Cornil, A.C.T. van Duin, D. van Duin, R. Smith, S.D. Kenny, J. Cornil, and D. Beljonne, Development of a ReaxFF potential for Ag/Zn/O and application to Ag deposition on ZnO, *Surf. Sci.*, 645(2016), p. 67.

[41] P. Tereshchuk and J.L.F. da Silva, Ethanol and water adsorption on close-packed 3d, 4d, and 5d transition-metal surfaces: A density functional theory investigation with van der Waals correction, *J. Phys. Chem. C*, 116(2012), No. 46, p. 24695.

[42] R. Shepard, S. Shepard, and M. Smeu, *Ab initio* investigation into the physisorption of noble gases on graphene, *Surf. Sci.*, 682(2019), p. 38.

[43] C.L. Peng, F.F. Min, L.Y. Liu, and J. Chen, A periodic DFT study of adsorption of water on sodium-montmorillonite (001) basal and (010) edge surface, *Appl. Surf. Sci.*, 387(2016), p. 308.

[44] Y. Xin, S.C. Hou, L. Xiang, and Y.X. Yu, Adsorption and substitution effects of Mg on the growth of calcium sulfate hemihydrate: An *ab initio* DFT study, *Appl. Surf. Sci.*, 357(2015), p. 1552.

[45] J. Liu, S.M. Wen, J.S. Deng, X.M. Chen, and Q.C. Feng, DFT study of ethyl xanthate interaction with sphalerite (110) surface in the absence and presence of copper, *Appl. Surf. Sci.*, 311(2014), p. 258.

[46] C.X. Cai, S.S. Wei, Z.P. Yin, J. Bai, W.W. Xie, Y. Li, F.W. Qin, Y. Su, and D.J. Wang, Oxygen vacancy formation and uniformity of conductive filaments in Si-doped Ta_2O_5 RRAM, *Appl. Surf. Sci.*, 560(2021), art. No. 149960.

[47] R.F.W. Bader, A quantum theory of molecular structure and its applications, *Chem. Rev.*, 91(1991), No. 5, p. 893.

[48] W. Tang, E. Sanville, and G. Henkelman, A grid-based Bader analysis algorithm without lattice bias, *J. Phys.: Condens. Matter*, 21(2009), No. 8, art. No. 084204.

[49] Y.D. Scherson, S.J. Aboud, J. Wilcox, and B.J. Cantwell, Surface structure and reactivity of rhodium oxide, *J. Phys. Chem. C*, 115(2011), No. 22, p. 11036.

[50] G. Henkelman, A. Arnaldsson, and H. Jónsson, A fast and robust algorithm for Bader decomposition of charge density, *Comput. Mater. Sci.*, 36(2006), No. 3, p. 354.

[51] Z. Cheng, B.J. Sherman, and C.S. Lo, Carbon dioxide activation and dissociation on ceria (110): A density functional theory study, *J. Chem. Phys.*, 138(2013), No. 1, art. No. 014702.

[52] N. Kuriakose, A. Mohan T, and P. Ghosh, Coverage dependent CO_2 activation on Ti_2C(111) surface: Effect of intrinsic subsurface Carbon vacancies, *Surf. Sci.*, 706(2021), art. No. 121798.

[53] E. Durgun, H. Manzano, R.J.M. Pellenq, and J.C. Grossman, Understanding and controlling the reactivity of the calcium silicate phases from first principles, *Chem. Mater.*, 24(2012), No. 7, p. 1262.

[54] M. Laanaiya, A. Bouibes, and A. Zaoui, Understanding why Alite is responsible of the main mechanical characteristics in Portland cement, *Cem. Concr. Res.*, 126(2019), art. No. 105916.

[55] G.J. Li, W.G. Hu, Y.N. Sun, J.Y. Xu, X. Cai, X.L. Cheng, Y.Y. Zhang, A.C. Tang, X. Liu, M.Y. Chen, W.P. Ding, and Y. Zhu, Reactivity and lability modulated by a valence electron moving in and out of 25-atom gold nanoclusters, *Angew. Chem.*, 132(2020), No. 47, p. 21321.

[56] S. Sarugaku, M. Arakawa, T. Kawano, and A. Terasaki, Electronic and geometric effects on chemical reactivity of 3d-transition-metal-doped silver cluster cations toward oxygen molecules, *J. Phys. Chem. C*, 123(2019), No. 42, p. 25890.

[57] A. Mascaraque, L.M.d.l Garza, and E.G. Michel, Electronic structure and reactivity of the Co/MoS_2(0001) interface, *Surf. Sci.*, 482-485(2001), p. 664.